



Efficient hydrogenation catalyst designing via preferential adsorption sites construction towards active copper



Dongcheng He^{a,d,1}, Tao Wang^{b,1}, Teng Li^a, Xinzhi Wang^{a,d}, Hongli Wang^{a,*}, Xingchao Dai^c, Feng Shi^{a,*}

^a State Key Laboratory for Oxo Synthesis and Selective Oxidation, Lanzhou Institute of Chemical Physics, Chinese Academy of Sciences, No. 18, Tianshui Middle Road, Lanzhou 730000, China

^b Center of Artificial Photosynthesis for Solar Fuels, School of Science, Westlake University, 18 Shilongshan Road, Hangzhou 310024, China

^c Leibniz-Institut für Katalyse e.V. an der Universität Rostock (LIKAT), Albert-Einstein-Str. 29a, Rostock 18059, Germany

^d University of Chinese Academy of Sciences, No. 19A, Yuquan Road, Beijing 100049, China

ARTICLE INFO

Article history:

Received 23 April 2021

Revised 22 June 2021

Accepted 29 June 2021

Available online 3 July 2021

Keywords:

Copper catalyst

Selective hydrogenation

Catalyst surface modification

Preferential adsorption

ABSTRACT

Based on the experimental and DFT calculation results, here for the first time we built preferential adsorption sites for nitroarenes by modification of the supported Cu catalysts surface with 1,10-phenanthroline (1,10-phen), by which the yield of aniline via reduction of nitroarene is enhanced three times. Moreover, a macromolecular layer was in-situ generated on supported Cu catalysts to form a stable macromolecule modified supported Cu catalyst, i.e., CuAlOx-M. By applying the CuAlOx-M, a wide variety of nitroarene substrates react smoothly to afford the desired products in up to > 99% yield with > 99% selectivity. The method tolerates a variety of functional groups, including halides, ketone, amide, and C = C bond moieties. The excellent catalytic performance of the CuAlOx-M can be attributed to that the 1,10-phen modification benefits the preferential adsorption of nitrobenzene and slightly weakens adsorption of aniline on the supported nano-Cu surface.

© 2021 Elsevier Inc. All rights reserved.

1. Introduction

Aniline and its derivatives are widely applied in the production of pharmaceuticals, agrochemicals, dyes, polymers, surfactants, and biologically active compounds [1]. Among the available preparation procedures [2,3], the selective reduction of nitroarenes with H₂ represents economical and environmentally friendly alternative for the synthesis of anilines [4]. In the past decades, a series of heterogeneous noble metal catalysts, such as Au [5–9], Ru [10–12], Pd [13–17], Pt [18–22], and Rh [5,23] et al. have been developed. However, high cost and limited availability of these precious metals [1,24–26] impeded the further industrial application. Besides, other reducible groups containing carbon–carbon or carbon-heteroatoms multiple bonds, carboxylic acid derivatives, halogen atoms or heterocycles, can be hydrogenated simultaneously in the presence of noble metal catalysts [27–29]. Therefore, great efforts have been paid for the application of non-noble metals such as Fe [1 30–37], Co [38–44], Ni [27–29,45–47], and Cu [48] in selective hydrogenation of nitro-compound with H₂.

Compared with Co, Ni, and Fe catalysts, Cu-based catalysts have better stability and safety. In this context, M. Gupta and co-workers developed Cu/N-CNTs using acetic acid as additive [49], and Kustov et al. also reported copper-based catalysts for the hydrogenation of dinitrobenzene at 145 °C [50,51]. Recently, Beller and co-workers made important progress and developed supported copper catalysts for general and chemo-selective hydrogenation of nitro compounds to amines in 66–96% yields under 5 MPa H₂ at 140 °C for 48 h [52]. Despite these achievements, relatively demanding reaction conditions such as acid additive, or high temperature (>140 °C) and long reaction time (up to 48 h), are usually required to obtain satisfactory results. Thus, it is appealing to develop a new method to enhance the catalytic activity of supported Cu catalyst and selectivity of desired products in nitroarene hydrogenation.

As is well known, enzymes has the characteristics of high efficiency, high specificity, mild reaction conditions and adjustability, which is one of the most remarkable catalysts in nature [53]. In the key process of enzyme catalysis, metals as the active center are coordinated with the macromolecular ligands in order to realize the coupling or transfer of electrons and energy [54]. Next, some weak interactions, including hydrogen bonds, van der Waals forces and so on, can promote the interaction between active site and reactant molecules [55]. Eventually, the high efficiency and

* Corresponding authors.

E-mail addresses: wanghl@licp.cas.cn (H. Wang), fshi@licp.cas.cn (F. Shi).

¹ These authors contributed equally to this work.

specificity of enzyme catalysis is achieved through construction of an energy-based preferential entrance channel, i.e., preferential adsorption sites to reactants, such as molecular recognition, functional groups effects, size or shape matching, energy advantages, etc [56]. Inspired by the basic principle of enzyme catalysis, mimic enzymes structure by surface modification of supported Cu catalysts would be a feasible strategy to enhance their catalytic activity for reduction of nitroarenes to amines. The crucial point about the surface macromolecular modification is constructing a selective adsorption and desorption surface which benefit preferential adsorption of nitroarenes and not influence desorption of aniline on the catalyst surface, thus it can obviously improve the catalytic performance in hydrogenation of nitroarenes to anilines. In this way, we envisioned that specific functional macromolecular modification of supported nano-Cu catalysts might tailor an effective Cu based catalyst for reduction of nitroarenes to anilines. In addition, strong adsorption is not conducive to substrate reaction and product desorption. Some weak interaction, for example hydrogen bonds, should be considered on process of adsorption or desorption for progress of catalytic reaction smoothly. For this reason, we chose N-heterocyclic ligands to study the interaction between organic ligands and CuAlOx.

Herein, we report that modification of supported nano-Cu catalyst with 1,10-phen, and also the in-situ generated macromolecular layer on catalyst surface, can significantly enhance its catalytic performance in selective reduction of nitro compounds to the corresponding amines (Fig. 1). The goal of this work is to show how to construct a heterogeneous catalyst via the inspiration from homogeneous catalysis, i.e., 1,10-phenatroline was used as the monomer to construct a stable “polymer ligand” or a “heterogeneous ligand” on the surface of supported copper catalysts (CuAlOx-M) for enhancing the catalytic performance of reduction of nitroarene substrates.

2. Experimental section

2.1. Catalyst preparation

All solvents and chemicals were obtained commercially and were used as received.

Preparation of CuAlOx. 0.15 g (0.6 mmol) of $\text{Cu}(\text{NO}_3)_2 \cdot 3\text{H}_2\text{O}$ and 4.3 g (11.4 mmol) of $\text{Al}(\text{NO}_3)_3 \cdot 9\text{H}_2\text{O}$ were added into 100 mL deionized water at room temperature in a 250 mL flask. Then, 40 mL of Na_2CO_3 solution (0.93 mol/L) was added dropwise into the solution under vigorous stirring and the mixture was stirred for a further 5 h at room temperature. The reaction mixture was centrifuged and washed with water to remove the base until the pH value of the aqueous solution was ≈ 7 . Next, the solid was dried at 100 °C for 12 h, calcined at 350 °C for 5 h, and then reduced under hydrogen flow at 350 °C for 3 h. Subsequently, black powder was obtained and denoted as CuAlOx.

Preparation of CuAlOx-M. A mixture of nitrobenzene (1 mmol) and 1,10-phenanthroline (0.1 mmol) was added to a glass tube which was placed in a 100 mL autoclave then the autoclave was sealed and exchanged with H_2 three times and reacted at 120 °C under 1.5 MPa H_2 for 8 h using CuAlOx as the catalyst. After the reaction, the autoclave then cooled down to room temperature. Next, the catalyst was separated from the reaction mixtures by centrifuging and washed with methylbenzene for three times. Finally, the catalyst dried in the air and named CuAlOx-M.

2.2. Catalyst characterization

For TEM investigations, the catalysts were dispersed in ethanol by ultrasonication and deposited on carbon-coated copper grids.

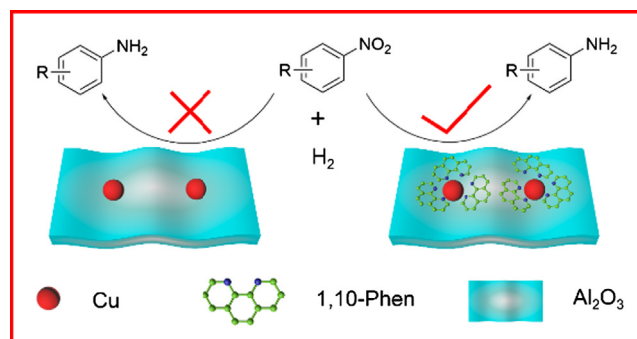


Fig. 1. Schematic diagram of nitrobenzene hydrogenation with CuAlOx.

TEM analysis was carried out on a FEI G2 F20 transmission electron microscope operating at 200 KeV.

XRD measurements were conducted by a STADIP automated transmission diffractometer (STOE) equipped with an incident beam curved germanium monochromator selecting Cu $K\alpha_1$ radiation and a 6° position sensitive detector (PSD). The XRD patterns are scanned in the 2θ range of $10\text{--}80^\circ$. For the data interpretation, the software WinXpov (STOE) and the database of Powder Diffraction File (PDF) of the International Centre of Diffraction Data (ICDD) were used.

XPS was obtained using a VG ES-CALAB 210 instrument equipped with a dual Mg/Al anode X-ray source, a hemispherical capacitor analyzer, and a 5 keV Ar + iron gun. The electron binding energy was referenced to the C 1s peak at 284.8 eV. The background pressure in the chamber was less than $10\text{--}7$ Pa. The peaks were fitted by Gaussian–Lorentzian curves after linear background subtraction. For quantitative analysis, the peak area was divided by the element-specific Scofield factor and the transmission function of the analyzer.

Thermogravimetric analysis (TGA) was performed on a METTLER TOLEDO simultaneous thermal analyzer in an air or N_2 atmosphere from 30 °C to 1000 °C and then maintained at 1000 °C for 60 min.

The contents of Cu in the catalysts were measured by inductively coupled plasma-atomic emission spectrometry (ICP-AES), using an Iris advantage Thermo Jarrel Ash device.

Nitrogen adsorption–desorption isotherms were measured at 77 K using American Quantachrome iQ2 automated gas sorption analyzer. The pore-size distribution was calculated by Barrett, Joyner, and Halenda (BJH) method from desorption isotherm.

Element analyses (EA) were performed with an Elementar VarioEL instrument.

Extended X-ray absorption fine structure (EXAFS) experiments were performed at the Beijing Synchrotron Radiation Facility (1W1B BSRF) in the Institute of High Energy Physics, Chinese Academy of Sciences with a storage ring energy of 2.5 GeV and a beam current between 150 and 250 mA. The Cu K edge absorbance of powder catalysts was measured in transmission geometry at room temperature. The energy was scanned from -200 eV below to 800 eV above the Cu K edge (8979 eV). EXAFS data analysis was carried out using ifffit analysis programs (<http://cars9.uchicago.edu/ifffit/>).

2.3. Catalytic performance test and procedure for recycling test

Catalytic Performance Test. A mixture of nitroarenes (1.0 mmol), catalyst (80 mg, 3.8 wt%) were added to a glass tube which was placed in a 100 mL autoclave. Then the autoclave was purged and charged with H_2 (1.5 MPa) three times. The reaction mixture

was stirred at 120 °C for 12 h. Then, the autoclave was cooled to room temperature and the pressure was carefully released. Subsequently, the reaction mixture was diluted with 10 mL toluene for quantitative analysis by GC-FID (Agilent 7890B-5977A).

Procedure for recycling test. The used catalyst of the N-doped carbon/CuAlOx was separated from the reaction mixtures by centrifuging, washed three times using methylbenzene. After being dried in air at room temperature, it was recovered and directly recharged into the autoclave for the next run.

3. Results and discussion

3.1. Screening of different ligands

At first, the hydrogenation of nitrobenzene was chosen as a model reaction to study the effects of organic ligands on the catalytic performance of supported Cu catalyst, i.e., CuAlOx (Table 1). As shown in Table 1, we can see that only 27% yield of aniline was obtained by CuAlOx lack of ligands and some ligands would inhibit the catalytic hydrogenation performance of copper, like pyridine and dipyridine, but some ligands, especially 1,10-phen, could significantly improve the catalytic performance with 81% yield (Table 1, Entry 1, 11). It should be noted that the catalytic performance was possibly related to the position or distance of two N-atoms in organic ligand.

3.2. DFT calculation

To validate our hypothesis further and get some insights into the different catalytic performances between clean Cu and Cu dispersed by 1,10-phen, we performed DFT studies to compare the adsorption energies of ArNO₂ and ArNH₂ on clean Cu and Cu dispersed by 1,10-phen.

It revealed that the adsorption of ArNO₂ on 1,10-phen_Cu (111) surface (−1.27 eV) was much stronger than on clean Cu (111) surface (−0.72 eV), which indicated a higher concentration of reactant on the surface and eventually enhanced activation of the reactant. The adsorption energy of ArNO₂ on 1,10-phen_Cu (111) surface (−1.27 eV) is also much stronger than 1,10-phenathroline adsorption energy (−1.01 eV). In this respect, full coverage of 1,10-phenathroline is not competitive at all in the presence of nitrobenzene. Therefore, we concluded that the partial precovering of 1,10-phenathroline on Cu surface is beneficial for nitrobenzene adsorption. Close inspections showed that the enhanced adsorption strength came from the formation of H-bonds between ArNO₂ and phen as shown in Fig. 2c. However, the adsorption of the ArNH₂ was slightly weaker on 1,10-phen_Cu (111) surface (−0.89 eV) than the clean Cu (111) surface (−0.91 eV). Therefore, we attributed the better performance of 1,10-phen_Cu catalyst in this reaction partially to the enhanced adsorption strength of reactant as well as desorption of product. Furthermore, we also evaluated the abilities of these two catalysts in H₂ activation, and the potential energy diagram, as well as structures of H₂ dissociation. The results were shown in Figs. S1 and S2. The 1,10-phen_Cu (111) surface has a higher H₂ dissociation energy barrier than Cu (111) surface, indicating the slightly weaker activity in H₂ activation.

To get more insights into the roles of different ligands in affecting the catalytic performances of Cu catalyst, we performed systematic DFT computations and all the computational details could be found in supporting information. As a start, we compared the adsorption energies of ArNO₂ (reactant) and ArNH₂ (product) as well as H₂ dissociation energy barriers on clean and different ligands modified Cu (111) surfaces (Fig. 3).

It revealed that each ligand had quite different effects on the adsorptions of reactant and product. As proposed in the Sabatier principle [57], the binding strength between the reaction intermediates and catalyst is essential in determining the catalytic performance of a catalyst. An optimal catalyst should have neither too strong nor too weak binding strength of reaction species, and ideally should be strong enough to activate the reactant but weak enough to release the product smoothly. Based on this principle, we can find that 1,10-phen modified Cu catalyst has such advantages, i.e., this catalyst has much stronger ArNO₂ adsorption strength than the clean Cu catalyst, indicating a strong ability in activating the reactant. Meanwhile, it has slight weaker adsorption strength of ArNH₂ than pure Cu, which indicates a more favorable desorption of the product. Similarly, 4,7-phen also enhances the adsorption strength of ArNO₂ while weakens the ArNH₂ adsorption despite that the enhancement is smaller compared with 1,10-phen.

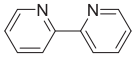
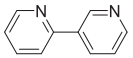
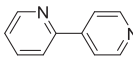
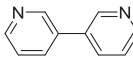
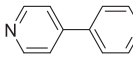
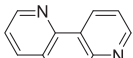
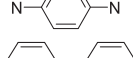
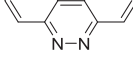
In contrary, ligand-2 weakens the adsorption of the ArNO₂, which will potentially reduce the ability in activating the reactant and eventually affect the performance of Cu catalyst. Additionally, we evaluated the effects of these ligands in H₂ activation, 4,7-phen and 1,10-phen have similar energy barriers with clean Cu catalyst in H₂ dissociation, whereas ligand-2 has much higher H₂ dissociation energy barrier indicating its potentially lower hydrogenation activity. Our simulations reveal that 1,10-phen has the most positive effect in ArNO₂ hydrogenation to ArNH₂ because of the enhanced ability in both reactant activation and product desorption, followed by 4,7-phen while 1,7-phen shows a negative effect. Indeed, all the simulated results are in reasonable agreement with the experimentally detected yields as listed in Table 2, i.e., 1,10-phen modified Cu has highest yield followed by ligand-3 and clean Cu, while 1,7-phen modified Cu catalyst has lowest yield. In addition, we found that 2,2'-Bipyridine has a quite different manners compared with 1,10-phenathroline. As shown in entry 5 of Table 2, the 2,2'-Bipyridine ligand enhanced the adsorptions of both reactant and product for nitrobenzene hydrogenation, which is different from that for 1,10-phenathroline. This result further confirms the special role of 1,10-phenathroline ligand in improving catalytic activities. The above experiment and DFT characterization results proved that our idea to manipulate the adsorption–desorption behavior of reactants and products on CuAlOx surface through introducing organic ligands was feasible.

3.3. Optimization of the reaction

In subsequent studies, we conducted optimization of the reaction conditions (Table 3). It was found that 99% nitrobenzene conversion and 99% aniline yield were achieved by using CuAlOx in the presence of 1,10-phen at 120 °C with 1.5 MPa H₂ for 12 h (Table 3, Entry 9). Noteworthy, the catalyst exhibited good reusability for at least 5 runs at full conversions by simple filtration using solvent without further addition of 1,10-phen (Fig. 4a). The recycling test of the catalyst has also been performed at relatively low conversions (17%–19%) within kinetic region, and it can be found that the catalyst could be reused at least 5 times without obvious loss in catalytic performance (Fig. 4b).

Moreover, we try to construct CuAlOx-M as catalyst for the reduction of nitroarenes (Table S5). Clearly, the best catalytic performance was obtained by treatment of CuAlOx with 1,10-phen in the presence of nitrobenzene for 8 h (Table S5, entry 11). With the macromolecular modification of supported Cu catalysts (CuAlOx-M) in hand, the scope and limitation of reduction of nitroarenes were investigated. As shown in Table 4, nitroarenes with both electron-withdrawing and electron-donating groups on the aromatic ring were effectively reacted to afford the desired products in 98–99% yields (2a–2i). It was found that the electronic and steric properties of the aryl substituents on the aromatic ring have little

Table 1
Catalytic hydrogenation of nitrobenzene with CuAlOx in the presence of different ligands.^a

Entry	Ligands	Conversion (%)	Selectivity (%)	Yield (%)
1	None	28	99	27
2		21	99	20
3		28	99	27
4		24	99	23
5		7	98	6
6		24	99	23
7		24	99	23
8		17	98	17
9		35	99	35
10		8	98	7
11		81	99	81

The data in Table 1 is the average of the results between the two groups of parallel reaction. ^a Nitrobenzene (1 mmol), CuAlOx (80 mg, 3.8 wt% Cu), ligand (10 mol%), toluene (4 mL), 1.5 MPa H₂, 150 °C, 1.5 h. ^b Conversions of nitrobenzene and yields of aniline were determined by GC-FID using diphenyl as the internal standard material. ^c Selectivity was determined by GC-MS.

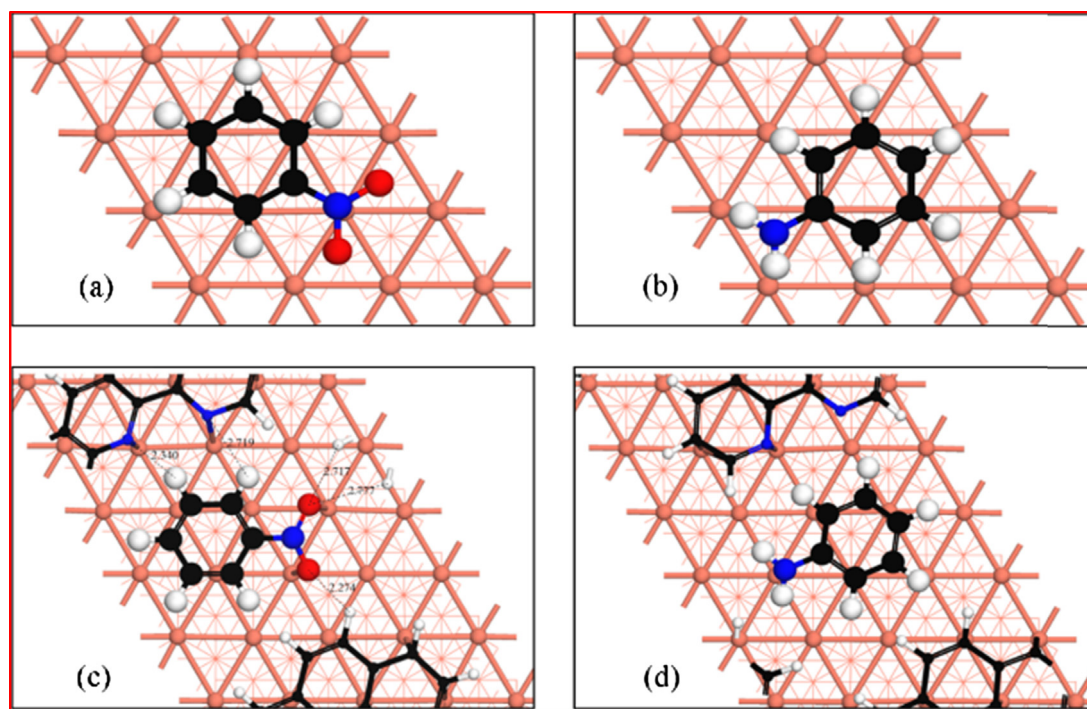


Fig. 2. Adsorption configurations of ArNO₂ and ArNH₂ on clean Cu (111) surfaces (a, b) and phen_Cu (111) surface (b, c), respectively. The numbers in (c) denote the lengths of H-bonds between ArNO₂ and phen. (H atom in white, C in black, O in red, N in blue and Cu in pink). (For interpretation of the references to colour in this figure legend, the reader is referred to the web version of this article.)

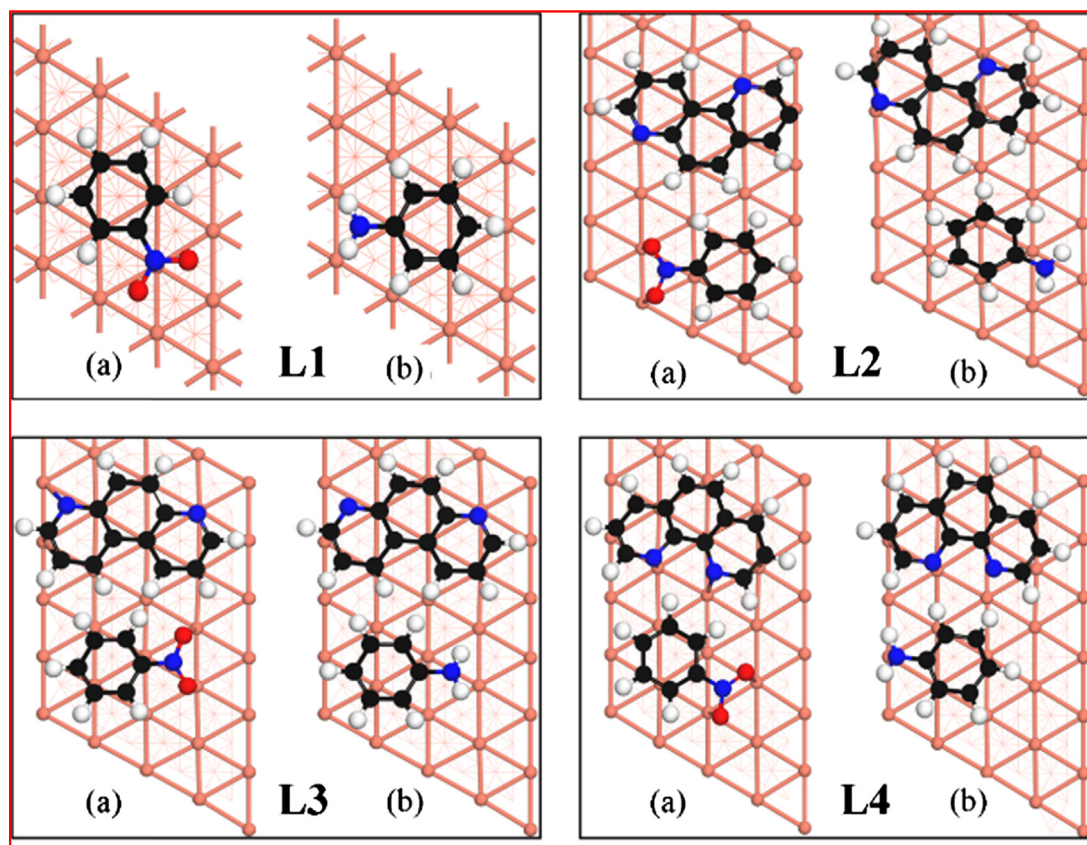
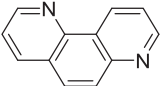
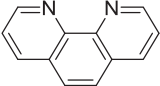
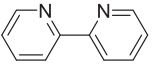


Fig. 3. The adsorption configurations of ArNO₂ and ArNH₂ on ligands doped Cu (111) surface.

Table 2

Adsorption energies (eV) of ArNO₂, ArNH₂ and H₂ dissociation energy barriers (eV) on different catalysts.

Entry	Catalyst	Ligands	Yield (%)	$E_{\text{ads}}(\text{ArNO}_2)/\text{eV}$	$E_{\text{ads}}(\text{ArNH}_2)/\text{eV}$	$E_{\text{a}}(\text{H}_2)/\text{eV}$
1	CuAlOx	None	27	-0.72	-0.91	0.45
2	CuAlOx		17	-0.57	-0.77	0.81
3	CuAlOx		35	-0.91	-0.83	0.48
4	CuAlOx		81	-1.27	-0.89	0.54
5	CuAlOx		28	-1.25	-1.49	0.50

effect on the observed reactivity and selectivity of the reaction. In addition, a variety of substrates containing sensitive functional groups, such as amino, halogen, ketones, esters, amides, and olefins was well-tolerated without being reduced to any substantial extent (2j–2v). Furthermore, dinitro-compounds were also successfully converted to the corresponding diamines in good yields (**2w** and **2x**).

3.4. Catalyst characterization

In order to investigate the relationship between structure and activity of CuAlOx catalyst after being used with the addition of

1,10-phen, a series of characterizations including X-ray photoelectron spectroscopy (XPS), X-ray powder diffraction (XRD), transmission electron microscope (TEM), Fourier transformed Cu K-edge EXAFS, inductively coupled plasma-atomic emission spectrometry (ICP-AES), elemental analysis (EA), and N₂ adsorption – desorption instruments have been performed for fresh CuAlOx catalyst and the CuAlOx being treated by ligands, nitrobenzene and H₂.

The XPS spectra presented two main peaks of fresh CuAlOx and treated CuAlOx catalysts at 933.1 eV and 953.1 eV, which were corresponding to the Cu 2p^{3/2} and 2p^{1/2} binding energy of Cu(II), respectively (Fig. 5A). Furthermore, the chemical state of Cu in CuAlOx catalysts was analyzed by Fourier transformed Cu K-edge

Table 3
Catalytic hydrogenation of nitrobenzene under different reaction conditions with 1,10-phenanthroline as ligand.^a

Entry	Reaction temperature (°C)	Reaction time (h)	Conversion (%) ^b	Selectivity (%) ^c	Yield (%) ^b
1	150	1.5	82	99	82
2	150	2	>99	99	>99
3	140	3	79	99	78
4	130	4	86	99	85
5	120	4	52	99	51
6	120	6	64	99	64
7	120	8	85	99	84
8	120	10	95	99	95
9	120	12	>99	99	>99
10	110	12	16	98	15

The data in Table 3 are the average of the results between the two groups of parallel reaction.

^aNitrobenzene (1 mmol), CuAlOx (80 mg, 3.8 wt% Cu), 1,10-phenanthroline (10 mol%), toluene (4 mL), 1.5 MPa H₂. ^bConversions of nitrobenzene and yields of aniline were determined by GC-FID using diphenyl as the internal standard material. ^cSelectivity was determined by GC-MS.

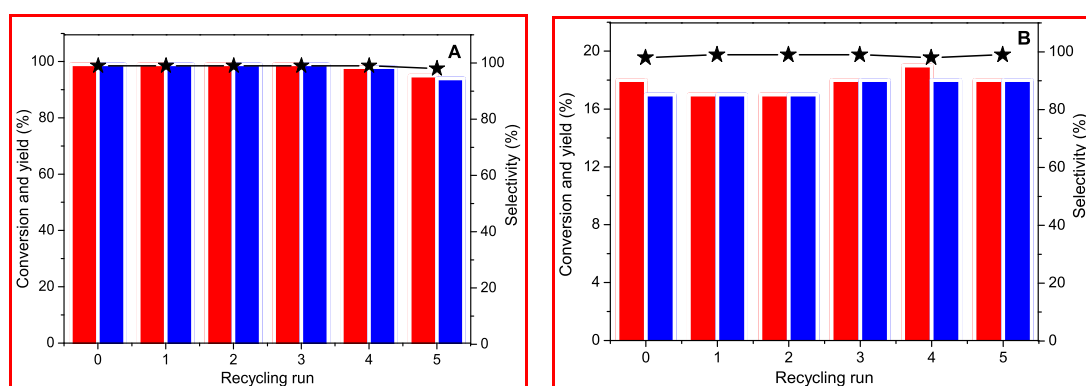


Fig. 4. Recycling test of CuAlOx-M for the hydrogenation of nitrobenzene. **(A)** at full conversion of nitrobenzene. **(B)** at relatively low conversions (17%–19%) of nitrobenzene. Reaction conditions: nitrobenzene (1 mmol), toluene (4 mL), 1.5 MPa H₂, 120 °C. All conversions of nitrobenzene and yields of aniline were determined by calibrated GC-FID using diphenyl as the internal standard material and selectivity was determined by GC-MS. (Conversion in red, yield in blue, selectivity in black). (For interpretation of the references to colour in this figure legend, the reader is referred to the web version of this article.)

EXAFS spectra (Fig. 5B). Clearly, two signal peaks at 1.56 and 2.23 Å were observed in CuAlOx catalysts samples being used for 1, 3 and 5 times. By comparing with standard spectra of Cu (curve a), Cu₂O (curve l) and CuO (curve m), the two peaks can be assigned to Cu-Cu coordination of metallic Cu (2.23 Å) and Cu-O coordination CuO (1.56 Å), respectively.

The surface C and N species of the catalysts were also analyzed by XPS (Fig. S3A, B). The XPS spectra of CuAlOx treated by 1,10-phen display a strong peak of N 1s at 399.7 eV and other ligands only a weak peak but not observable in fresh CuAlOx (Fig. S3C).

In XRD diffraction patterns, the fresh Al₂O₃ samples (Fig. 5A, curve a) show characteristic diffraction peaks of Al₂O₃ at 14.1°, 28.1°, 37.9°, 45.9° and 66.2° (PDF#46–1131). The CuAlOx samples (Fig. 6A, curve b) showed XRD reflections at 43.3°, 50.4°, and 74.1°, which can be respectively assigned to (111), (200) and (220) reflection lines of metallic Cu (PDF#99–0034). Notably, the catalyst of CuAlOx treated by 1,10-phen (Fig. 6A, curve c) exhibited a new diffraction peak located at 18.0°, which was the typical diffraction peak of N-doped carbon (PDF#51–2183) [58]. It can be inferred that the peak of N 1s at 399.7 eV in XPS came from the newly formed N-doped carbon. It was noticeable that this peak was also observed in used catalysts of 1, 3 and 5 times (Fig. 6A, curves d, e, f) and the diffraction patterns intensity increased gradually. Obviously, the intensity at 18.0° increased gradually with the extension of reaction time (Fig. 6B, curves a–f). These results sug-

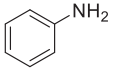
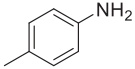
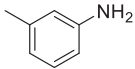
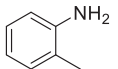
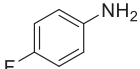
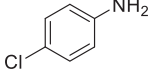
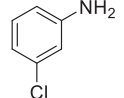
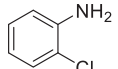
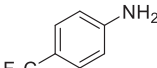
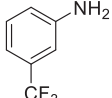
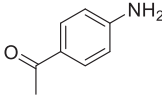
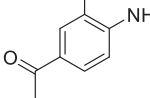
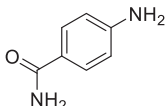
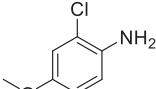
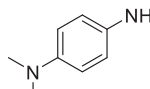
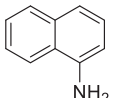
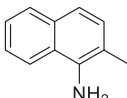
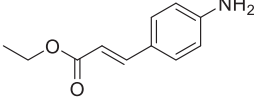
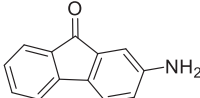
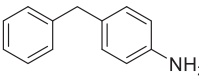
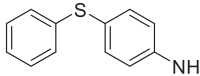
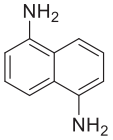
gested that N-doped carbon not only can be preserved after 5th runs, but also its crystal form became better and better as time extends, which may explain the reason why the catalyst good recyclability after the first run.

According to the N₂ adsorption–desorption isotherms, the formation of a mesoporous structure of the fresh CuAlOx catalyst was observed (Table S1). Clearly, it was composed of pores with radius of 2.8 nm and 6.3 nm. The results showed that the porous structure partly disappeared after the treatment of fresh catalyst under different conditions, which should be attributed to the formation of layered carbon, resulting in clogged meso-pores of the fresh CuAlOx catalyst. The BET surface areas of the fresh and treated catalysts (Table S1) were 137.0–249.5 m²·g⁻¹.

As can be seen from Fig. 7, TEM images of fresh CuAlOx mainly contain a lattice fringe of *d* = 0.21 nm for Cu (111) (Fig. 7a). In consideration of metallic copper in TEM characterizations, the surface Cu (II) observed in XPS should be attributed to the air oxidation of surface Cu (0) [52]. Compared with fresh CuAlOx, the TEM images of treated CuAlOx on the surface of nano-Cu appeared a lattice fringe of *d* = 0.28 nm that was considered to be the characteristic lattice fringe of layered carbon (Fig. 7b, c, d). Thus, the TEM image further confirmed the observations and conclusions from XPS, EXAFS, and XRD as well as N₂ adsorption–desorption analysis.

Subsequently, the loadings of N-doped carbon were determined by elemental analysis (EA). The results showed that the contents of

Table 4
Catalytic hydrogenation of various aromatic nitro compounds.^a

$\text{R-NO}_2 \xrightarrow[\text{1.5 MPa H}_2, \text{120 } ^\circ\text{C}]{\text{CuAlOx-M}} \text{R-NH}_2$	
1	2
	
2a, >99% (>99%)	2b, >99% (>99%)
	
2c, >99% (>99%)	2d, >99% (>99%)
	
2e, >99% (>99%)	2f, >99% (>99%)
	
2g, >99% (>99%)	2h, >99% (>99%)
	
2i, >99% (>99%)	2j, >99% (>99%)
	
2k, >99% (98%)	2l, >99% (98%)
	
2m, >99% ^b (98%)	2n, >99% (>99%)
	
2o, >99% (>99%)	2p, >99% (>99%)
	
2q, >99% (>99%)	2r, >99% (>99%)
	
2s, >99% (>99%)	
	
2t, >99% (>99%)	2u, >99% (>99%)
	
2v, >99% (>99%)	
	
2w, >99% ^c (>99%)	2x, 99% (99%) ^d

^aAll conversions and yields were determined by calibrated GC-FID using diphenyl as the internal standard material. The conversions of nitro compounds were showed below the structural formula and yields of anilines were given in parentheses. Reaction conditions: 1 mmol of substrates, 80 mg of CuAlOx-M, 1.5 MPa H₂, 4 mL toluene, 120 °C, 14 h. ^b 17 h. ^c 16 h. ^d 20 h.

C, H and N was 9–15 wt% (Table S2). According to the analysis, the 0.7–1.5 wt% N and 6.6–10.6 wt% C (Table S2), can be considered to confirm the ratio of N and C in 1,10-phen, excluding the residual of solvent and adsorption of CO₂ from the air in the drying process. EA

analysis showed that the nitrogen and carbon contents in catalyst were consistent with the ratio of N and C in 1,10-phen. Therefore, we speculate that the N-doped layer carbon is probably a 1,10-phenanthroline polymer. In the above discussion, with the extension

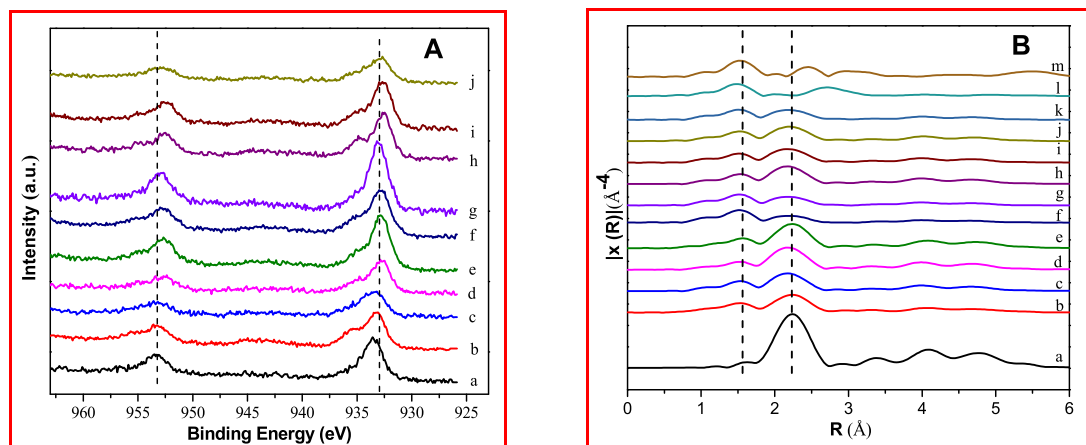


Fig. 5. (A) Cu 2p XPS spectra of the catalysts. a, CuAlOx; b, CuAlOx reused 1 time; c, CuAlOx reused 3 times; d, CuAlOx reused 5 times; e, CuAlOx reaction for 4 h; f, CuAlOx reaction for 8 h; g, CuAlOx reaction for 12 h; h, CuAlOx reaction for 16 h; i, CuAlOx reaction for 20 h; j, CuAlOx reaction for 24 h. (B) Fourier transform (FT) of Cu K-edge EXAFS. a, Cu; b, CuAlOx; c, CuAlOx reused 1 time; d, CuAlOx reused 3 times; e, CuAlOx reused 5 times; f, CuAlOx reaction for 4 h; g, CuAlOx reaction for 8 h; h, CuAlOx reaction for 12 h; i, CuAlOx reaction for 16 h; j, CuAlOx reaction for 20 h; k, CuAlOx reaction for 24 h; l, Cu₂O; m, CuO.

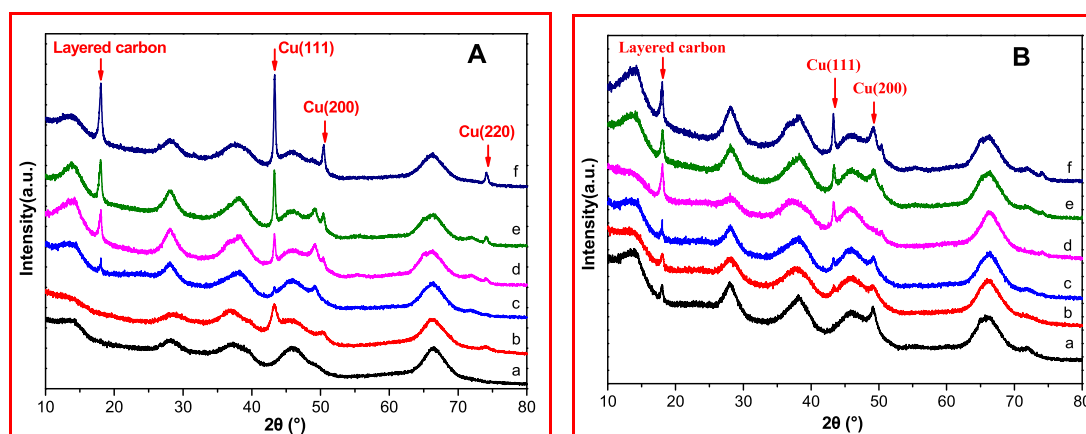


Fig. 6. (A) XRD patterns of the samples. Al₂O₃ (curve a); CuAlOx (curve b); CuAlOx after reaction of nitrobenzene reduction with 1,10-phenanthroline and H₂ for 12 h (curve c); CuAlOx reused 1 time (curve d); CuAlOx reused 3 times (curve e); CuAlOx reused 5 times (curve f). (B) XRD patterns of the CuAlOx samples after reaction of nitrobenzene reduction with 1,10-phenanthroline and H₂ for 4 h (curve a); 8 h (curve b); 12 h (curve c); 16 h (curve d); 20 h (curve e); 24 h (curve f).

of reaction time or the recycling times, XRD and TEM results showed that the crystal lattice of the N-doped carbon was better and clearer gradually. However, the weight of N-doped carbon decreased in EA, which may be the fact that extra 1,10-phen molecules deviate from the surface of the catalyst during the process of macromolecular from disordered to ordered state.

The copper contents of catalysts and reaction solution were tested by ICP-AES, including reused catalysts and treated catalysts for different times (Tables S3–S4). It was found that the Cu-load of fresh CuAlOx and CuAlOx-M respectively was 3.8 wt% and 3.5 wt%. The data of 3.5 wt%, 3.5 wt%, 3.4 wt% was observed for CuAlOx-M catalysts after the first, third and fifth runs. The copper contents in the solution after each cycle were tested by ICP-AES. The copper content in the solution after each recycle was below the detection limit of the instrument (0.1 ppm) at the 1st to 5th runs, which indicated good stability of the CuAlOx-M catalyst (Table S4).

4. Conclusions

In conclusion, we have developed an effective method for enhancing the catalytic performance of supported nano-Cu catalyst by modification with organic ligand on their surface. The in-situ generated macromolecular modified supported copper catalyst, i.e., CuAlOx-M, exhibits good catalytic performance in selective hydrogenation of nitro compounds to amines with up to 99% yield under mild conditions. A series of characterizations and DFT study results show that the enhanced catalytic performance of supported nano-Cu catalyst could be attributed to that the modification with 1,10-phen build preferential adsorption sites to nitroarenes and slightly weaken the adsorption of aniline on the catalyst surface. This work offers an effective methodology for the precise regulation of the catalytic performance of heterogeneous catalysts on molecular level.

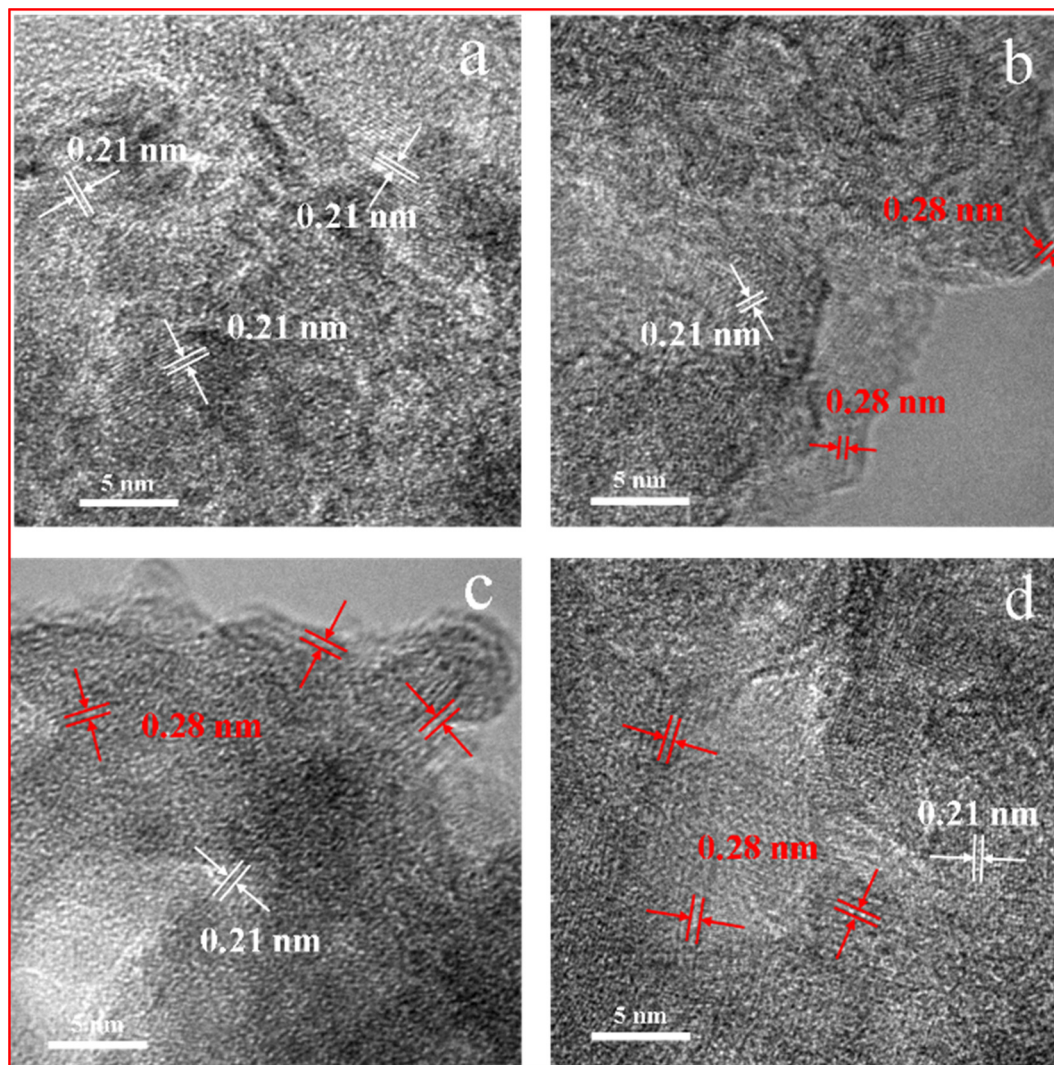


Fig. 7. TEM images of catalysts. a, CuAlOx; b, N-doped carbon/CuAlOx reused 1 time; c, N-doped carbon/CuAlOx reused 3 times; d, N-doped carbon/CuAlOx reused 5 times.

Author contributions

The manuscript was written through contributions of all authors. All authors have given approval to the final version of the manuscript.

Declaration of Competing Interest

The authors declare that they have no known competing financial interests or personal relationships that could have appeared to influence the work reported in this paper.

Acknowledgment

Financial supports from the NSFC (21925207), National Key Research and Development Program of China (2017YFA0403103), the Youth Innovation Promotion Association of CAS (2019409), the 'Light of West China' Program, Key Research Program of Frontier Sciences of CAS (QYZDJSSW-SLH051) of CAS, LICP Cooperation Foundation for Young Scholars (HZJJ20-01, HZJJ20-02) are gratefully acknowledged. We thank Dr. Shuai Chen (Institute of Coal Chemistry, CAS) for helping us to perform the TEM characterization and Prof. Dr. Lirong Zheng (Institute of High Energy Physics, CAS)

for helping us to perform the EXAFS (1W1B BSRF) analysis. We thank Westlake University HPC Center for computation support.

Appendix A. Supplementary material

The supporting information is available free of charge online, including experimental details; XPS spectra; TEM images; XRD patterns; the data of ICP-AES, EA and N₂ adsorption–desorption. Supplementary data to this article can be found online at <https://doi.org/10.1016/j.jcat.2021.06.025>.

References

- [1] R.V. Jagadeesh, A.-E. Surkus, H. Junge, M.-M. Pohl, J. Radnik, J. Rabeah, H. Huan, V. Schuenemann, A. Brueckner, M. Beller, Nanoscale Fe₂O₃-based catalysts for selective hydrogenation of nitroarenes to anilines, *Science* 342 (2013) 1073–1076.
- [2] S. Ahammed, A. Saha, B.C. Ranu, Hydrogenation of azides over copper nanoparticle surface using ammonium formate in water, *J. Org. Chem.* 76 (2011) 7235–7239.
- [3] Y. Aubin, C. Fischmeister, C.M. Thomas, J.-L. Renaud, Direct amination of aryl halides with ammonia, *Chem. Soc. Rev.* 39 (2010) 4130–4145.
- [4] H.-U. Blaser, H. Steiner, M. Studer, Selective catalytic hydrogenation of functionalized nitroarenes: an update, *ChemCatChem* 1 (2009) 210–221.
- [5] S. Sharma, P. Yamini, Das, Hydrogenation of nitroarenes to anilines in a flow reactor using polystyrene supported rhodium in a catalyst-cartridge (Cart-Rh@PS), *New J. Chem.* 43 (2019) 1764–1769.

- [6] M. Boronat, P. Concepcion, A. Corma, S. Gonzalez, F. Illas, P. Serna, A molecular mechanism for the chemoselective hydrogenation of substituted nitroaromatics with nanoparticles of gold on TiO₂ catalysts: A cooperative effect between gold and the support, *J. Am. Chem. Soc.* 129 (2007) 16230–16237.
- [7] L. Wang, E. Guan, J. Zhang, J. Yang, Y. Zhu, Y. Han, M. Yang, C. Cen, G. Fu, B.C. Gates, F.-S. Xiao, Single-site catalyst promoters accelerate metal-catalyzed nitroarene hydrogenation, *Nat. Commun.* 9 (2018) 1362.
- [8] L. Qin, G. Zeng, C. Lai, D. Huang, C. Zhang, M. Cheng, H. Yi, X. Liu, C. Zhou, W. Xiong, F. Huang, W. Cao, Synthetic strategies and application of gold-based nanocatalysts for nitroaromatics reduction, *Sci. Total Environ.* 652 (2019) 93–116.
- [9] J. Zhao, H. Yuan, J. Li, W. Bing, W. Yang, Y. Liu, J. Chen, C. Wei, L. Zhou, S. Fang, Effects of preparation parameters of NiAl oxide-supported Au catalysts on nitro compounds chemoselective hydrogenation, *ACS Omega* 5 (2020) 7011–7017.
- [10] B.J. Zuo, Y. Wang, Q.L. Wang, J.L. Zhang, N.Z. Wu, L.D. Peng, L.L. Gui, X.D. Wang, R.M. Wang, D.P. Yu, An efficient ruthenium catalyst for selective hydrogenation of ortho-chloronitrobenzene prepared via assembling ruthenium and tin oxide nanoparticles, *J. Catal.* 222 (2004) 493–498.
- [11] P. Zhang, F. Zhu, X. Tan, W. Li, S. Xu, P. Zhang, C. Wei, S. Miao, One-step synthesis of Ru/montmorillonite composite from gel system of RuCl₃-Na₂O-ZnO-Al₂O₃-SiO₂-F-H₂O and applications in nitrobenzene update hydrogenation catalysis, *Appl Clay Sci* 166 (2018) 207–213.
- [12] J. Zhang, L. Pei, J. Wang, P. Zhu, X. Gu, Z. Zheng, Differences in the selective reduction mechanism of 4-nitroacetophenone catalysed by rutile- and anatase-supported ruthenium catalysts, *Catal. Sci. Technol.* 10 (2020) 1518–1528.
- [13] J.-H. Lyu, X.-B. He, C.-S. Lu, L. Ma, Q.-F. Zhang, F. Feng, X.-N. Li, J.-G. Wang, The promoting role of minor amount of water in solvent-free hydrogenation of halogenated nitrobenzenes, *Chin. Chem. Lett.* 25 (2014) 205–208.
- [14] S. Sadjadi, M. Akbari, B. Leger, E. Monflier, M.M. Heravi, Eggplant-derived biochar-halloysite nanocomposite as supports of Pd nanoparticles for the catalytic hydrogenation of nitroarenes in the presence of cyclodextrin, *ACS Sustain. Chem. Eng.* 7 (2019) 6720–6731.
- [15] S. Sadjadi, M.M. Heravi, Pd@tetrahedral hollow magnetic nanoparticles coated with N-doped porous carbon as an efficient catalyst for hydrogenation of nitroarenes, *Appl. Organomet. Chem.* 33 (2019) e5229.
- [16] Y. Ma, Y. Ren, Y. Zhou, W. Liu, W. Baaziz, O. Ersen, C. Pham-Huu, M. Greiner, W. Chu, A. Wang, T. Zhang, Y. Liu, High-density and thermally stable palladium single-atom catalysts for chemoselective hydrogenations, *Angew. Chem. Int. Ed.* 59 (2020) 21613–21619.
- [17] J. Zhang, L. Wang, F. Chen, F.-S. Xiao, Efficient adjustment of product selectivity using controllable Pd nanoparticles in nitroarene hydrogenation, *Particuology* 48 (2020) 13–18.
- [18] P. Jing, T. Gan, H. Qi, B. Zheng, X. Chu, G. Yu, W. Yan, Y. Zou, W. Zhang, G. Liu, Synergism of Pt nanoparticles and iron oxide support for chemoselective hydrogenation of nitroarenes under mild conditions, *Chin. J. Catal.* 40 (2019) 214–222.
- [19] M. Liu, X. Mo, Y. Liu, H. Xiao, Y. Zhang, J. Jing, V.L. Colvin, W.W. Yu, Selective hydrogenation of o-chloronitrobenzene using supported platinum nanoparticles without solvent, *Appl. Catal., A: Chem.* 439 (2012) 192–196.
- [20] R. Xie, X. Cao, Y. Pan, H. Gu, Synthesis of Pt nanocatalysts for selective hydrogenation of ortho-halogenated nitrobenzene, *Sci China Chem* 58 (2015) 1051–1055.
- [21] Y. Ren, Y. Tang, L. Zhang, X. Liu, L. Li, S. Miao, D.S. Su, A. Wang, J. Li, T. Zhang, Unraveling the coordination structure-performance relationship in Pt-1/Fe₂O₃ single-atom catalyst, *Nat. Commun.* 10 (2019) 4500.
- [22] M. Macino, A.J. Barnes, R. Qu, E.K. Gibson, D.J. Morgan, S.J. Freakley, N. Dimitratos, C.J. Kiely, X. Gao, A.M. Beale, D. Bethell, Q. He, M. Sankar, G.J. Hutchings, S.M. Althabhan, Tuning of catalytic sites in Pt/TiO₂ catalysts for the chemoselective hydrogenation of 3-nitrostyrene, *Nat. Catal.* 2 (2019) 873–881.
- [23] H. Tian, J. Zhou, Y. Li, Y. Wang, L. Liu, Y. Ai, Z.-N. Hu, J. Li, R. Guo, Z. Liu, H.-B. Sun, Q. Liang, Rh catalyzed selective hydrogenation of nitroarenes under mild conditions: understanding the functional groups attached to the nanoparticles, *ChemCatChem* 11 (2019) 5543–5552.
- [24] S. Anantharaj, P.E. Karthik, B. Subramanian, S. Kundu, Pt nanoparticle anchored molecular self-assemblies of DNA: An extremely stable and efficient HER electrocatalyst with ultralow Pt content, *ACS Catal.* 6 (2016) 4660–4672.
- [25] L. Geng, M. Zhang, W. Zhang, M. Jia, W. Yan, G. Liu, Rational design of carbon support to prepare ultrafine iron oxide catalysts for air oxidation of alcohols, *Catal. Sci. Technol.* 5 (2015) 3097–3102.
- [26] Y. Sui, S. Liu, T. Li, Q. Liu, T. Jiang, Y. Guo, J.-L. Luo, Atomically dispersed Pt on specific TiO₂ facets for photocatalytic H₂ evolution, *J. Catal.* 353 (2017) 250–255.
- [27] P. Lara, K. Philippot, The hydrogenation of nitroarenes mediated by platinum nanoparticles: an overview, *Catal. Sci. Technol.* 4 (2014) 2445–2465.
- [28] W. Shi, B. Zhang, Y. Lin, Q. Wang, Q. Zhang, D.S. Su, Enhanced chemoselective hydrogenation through tuning the interaction between Pt nanoparticles and carbon supports: insights from identical location transmission electron microscopy and X-ray photoelectron spectroscopy, *ACS Catal.* 6 (2016) 7844–7854.
- [29] G. Vile, D. Albani, N. Almora-Barrios, N. Lopez, J. Perez-Ramirez, Advances in the design of nanostructured catalysts for selective hydrogenation, *ChemCatChem* 8 (2016) 21–33.
- [30] J. Chen, Y. Yao, J. Zhao, Y. Zhao, Y. Zheng, M. Li, Q. Yang, A highly active non-precious metal catalyst based on Fe-N-C@CNTs for nitroarene reduction, *RSC Adv.* 6 (2016) 96203–96209.
- [31] R.V. Jagadeesh, T. Stemmler, A.-E. Surkus, H. Junge, K. Junge, M. Beller, Hydrogenation using iron oxide-based nanocatalysts for the synthesis of amines, *Nat. Protoc.* 10 (2015) 548–557.
- [32] H. Niu, J. Lu, J. Song, L. Pan, X. Zhang, L. Wang, J.-J. Zou, Iron oxide as a catalyst for nitroarene hydrogenation: important role of oxygen vacancies, *Ind. Eng. Chem. Res.* 55 (2016) 8527–8533.
- [33] B. Sahoo, D. Formenti, C. Topf, S. Bachmann, M. Scalone, K. Junge, M. Beller, Biomass-derived catalysts for selective hydrogenation of nitroarenes, *ChemSusChem* 10 (2017) 3035–3039.
- [34] S. Xu, D. Yu, S. Liao, T. Ye, H. Sheng, Nitrogen-doped carbon supported iron oxide as efficient catalysts for chemoselective hydrogenation of nitroarenes, *RSC Adv.* 6 (2016) 96431–96435.
- [35] Y. Wang, R. Qin, Y. Wang, J. Ren, W. Zhou, L. Li, J. Ming, W. Zhang, G. Fu, N. Zheng, Chemoselective hydrogenation of nitroaromatics at the nanoscale iron (III)-OH-platinum interface, *Angew. Chem. Int. Ed.* 59 (2020) 12736–12740.
- [36] A.J. MacNair, T. Ming-Ming, J.E. Nelson, G.U. Sloan, A. Ironmonger, S.P. Thomas, Iron-catalysed, general and operationally simple formal hydrogenation using Fe(OTf)₃ and NaBH₄, *Org. Biomol. Chem.* 12 (2014) 5082–5088.
- [37] Y. Duan, X. Dong, T. Song, Z. Wang, J. Xiao, Y. Yuan, Y. Yang, Hydrogenation of functionalized nitroarenes catalyzed by single-phase pyrite FeS₂ nanoparticles on N, S-codoped porous carbon, *ChemSusChem* 12 (2019) 4636–4644.
- [38] F.A. Westerhaus, R.V. Jagadeesh, G. Wienhoefer, M.-M. Pohl, J. Radnik, A.-E. Surkus, J. Rabeah, K. Junge, H. Junge, M. Nielsen, A. Brueckner, M. Beller, Heterogenized cobalt oxide catalysts for nitroarene reduction by pyrolysis of molecularly defined complexes, *Nat. Chem.* 5 (2013) 537–543.
- [39] R.V. Jagadeesh, T. Stemmler, A.-E. Surkus, M. Bauer, M.-M. Pohl, J. Radnik, K. Junge, H. Junge, A. Brueckner, M. Beller, Cobalt-based nanocatalysts for green oxidation and hydrogenation processes, *Nat. Protoc.* 10 (2015) 916–926.
- [40] F. Chen, B. Sahoo, C. Kreyenschulte, H. Lund, M. Zeng, L. He, K. Junge, M. Beller, Selective cobalt nanoparticles for catalytic transfer hydrogenation of N-heteroarenes, *Chem. Sci.* 8 (2017) 6239–6246.
- [41] T. Song, P. Ren, Y. Duan, Z. Wang, X. Chen, Y. Yang, Cobalt nanocomposites on N-doped hierarchical porous carbon for highly selective formation of anilines and imines from nitroarenes, *Green Chem.* 20 (2018) 4629–4637.
- [42] H. Li, C. Cao, J. Liu, Y. Shi, R. Si, L. Gu, W. Song, Cobalt single atoms anchored on N-doped ultrathin carbon nanosheets for selective transfer hydrogenation of nitroarenes, *Sci. China Mater.* 62 (2019) 1306–1314.
- [43] O.W. Brown, C.O. Henke, Catalytic preparation of aniline II, *J. Phys. Chem.* 26 (1922) 272–287.
- [44] R. Raja, V.B. Golovko, J.M. Thomas, A. Berenguer-Murcia, W.Z. Zhou, S.H. Xie, B. F.G. Johnson, Highly efficient catalysts for the hydrogenation of nitro-substituted aromatics, *Chem. Commun.* 2026–2028 (2005).
- [45] X. Liu, X. Ma, S. Liu, Y. Liu, C. Xia, Metal fluoride promoted catalytic hydrogenation of aromatic nitro compounds over RANEY (R) Ni, *RSC Adv.* 5 (2015) 36423–36427.
- [46] M. Studer, S. Neto, H.U. Blaser, Modulating the hydroxylamine accumulation in the hydrogenation of substituted nitroarenes using vanadium-promoted RNI catalysts, *Top. Catal.* 13 (2000) 205–212.
- [47] C.S. Lu, J.H. Lv, L. Ma, Q.F. Zhang, F. Feng, X.N. Li, Highly selective hydrogenation of halonitroaromatics to aromatic haloamines by ligand modified Ni-based catalysts, *Chin. Chem. Lett.* 23 (2012) 545–548.
- [48] Z. Yin, Y. Xiao, X. Wan, Y. Jiang, G. Chen, Q. Shi, S. Cao, High photocatalytic activity of Cu₂O embedded in hierarchically hollow SiO₂ for efficient chemoselective hydrogenation of nitroarenes, *J. Mater. Sci.* 56 (2021) 3874–3886.
- [49] G. Kour, M. Gupta, B. Vishwanathan, K. Thirunavukkarasu, (Cu/NCNTs): a new high temperature technique to prepare a recyclable nanocatalyst for four component pyridine derivative synthesis and nitroarenes reduction, *New J. Chem.* 40 (2016) 8535–8542.
- [50] E.V. Shuvalova, O.A. Kirichenko, G.I. Kapustin, L.M. Kustov, Silica-supported copper nanoparticles as efficient catalysts for the liquid-phase selective hydrogenation of p-dinitrobenzene by molecular hydrogen, *Russ. Chem. Bull.* 65 (2016) 2850–2854.
- [51] A.A. Shesterkina, E.V. Shuvalova, O.A. Kirichenko, A.A. Strelkova, V.D. Nissenbaum, G.I. Kapustin, L.M. Kustov, Application of silica-supported Fe-Cu nanoparticles in the selective hydrogenation of p-dinitrobenzene to p-phenylenediamine, *Russ. J. Phys. Chem. A* 91 (2017) 201–204.
- [52] W. Li, X. Cui, K. Junge, A.E. Surkus, C.R. Kreyenschulte, S. Bartling, M. Beller, General and chemoselective copper oxide catalysts for hydrogenation reactions, *ACS Catal.* 9 (2019) 4302–4307.
- [53] B.M. Bonk, J.W. Weis, B. Tidor, Machine learning identifies chemical characteristics that promote enzyme catalysis, *J. Am. Chem. Soc.* 141 (2019) 4108–4118.
- [54] M.J. Wiester, P.A. Ulmann, C.A. Mirkin, Enzyme mimics based upon supramolecular coordination chemistry, *Angew. Chem. Int. Ed.* 50 (2011) 114–137.
- [55] A. Warshel, P.K. Sharma, M. Kato, Y. Xiang, H. Liu, M.H.M. Olsson, Electrostatic basis for enzyme catalysis, *Chem. Rev.* 106 (2006) 3210–3235.
- [56] Y. Zhang, H. Hess, Toward rational design of high-efficiency enzyme cascades, *ACS Catal.* 7 (2017) 6018–6027.
- [57] A.J. Medford, A. Vojvodic, J.S. Hummelshoj, J. Voss, F. Abild-Pedersen, F. Studt, T. Bligaard, A. Nilsson, J.K. Nørskov, From the Sabatier principle to a predictive theory of transition-metal heterogeneous catalysis, *J. Catal.* 328 (2015) 36–42.
- [58] Y. Wu, T. Wang, H. Wang, X. Wang, X. Dai, F. Shi, Active catalyst construction for CO₂ recycling via catalytic synthesis of N-doped carbon on supported Cu, *Nat. Commun.* 10 (2019) 2599.